Title

Clinical, Pathologic, and Mutational Spectrum of Dystroglycanopathy Caused by LARGE Mutations

Journal

Journal of Neuropathology & Experimental Neurology, 73(5)

ISSN

0022-3069

Authors

Meilleur, Katherine G
Zukosky, Kristen
Medne, Livija
et al.

Publication Date

2014-05-01

DOI

10.1097/nen.0000000000000065

Peer reviewed

Published in final edited form as:

J Neuropathol Exp Neurol. 2014 May ; 73(5): 425–441. doi:10.1097/NEN.0000000000000065.

Clinical, Pathological and Mutational Spectrum of Dystroglycanopathy Due to *LARGE* Mutations

Katherine G. Meilleur, PhD[1], **Kristen Zukosky, MS**[2], **Livija Medne, MS**[3], **Pierre Fequiere, MD**[4], **Nina Powell-Hamilton, MD**[5], **Thomas L. Winder, PhD**[6], **Abdulaziz Alsaman, MD**[7,8], **Ayman W. El-Hattab, MD**[8,9], **Jahannaz Dastgir, DO**[2], **Ying Hu, MS**[2], **Sandra Donkervoort, MS**[2], **Jeffrey A. Golden, MD**[10,11], **Ralph Eagle, MD**[12], **Richard Finkel, MD**[13], **Mena Scavina, MD**[5], **Ian C. Hood, MD**[14], **Lucy B. Rorke-Adams, MD**[3], and **Carsten G. Bönnemann, MD**[2]

[1]National Institute of Nursing Research, Bethesda, MD

[2]National Institute of Neurological Disorders and Stroke, Bethesda, MD

[3]Children's Hospital of Philadelphia, Philadelphia, PA

[4]Department of Pediatrics, Division of Pediatric Neurology, University of Alabama at Birmingham, Birmingham, AL

[5]Nemours Children's Hospital, Wilmington, DE

[6]Prevention Genetics, Marshfield, WI

[7]Pediatric Neurology Department, National Neuroscience Institute, King Fahad Medical City, Riyadh, Kingdom of Saudi Arabia

[8]College of Medicine, King Saud bin Abdulaziz University for Health Sciences, Riyadh, Kingdom of Saudi Arabia

[9]Division of Medical Genetics, Department of Pediatrics, The Children's Hospital, King Fahad Medical City, Riyadh, Kingdom of Saudi Arabia

[10]Department of Pathology, Brigham and Women's Hospital, Boston, MA

[11]Harvard Medical School, Boston, MA

[12]Department of Pathology, Wills Eye Institute, Thomas Jefferson University, Philadelphia, PA

[13]Nemours Children's Hospital, Orlando, FL

[14]Medical Examiner's Office, Mount Holly, NJ.

Abstract

Dystroglycanopathies are a subtype of congenital muscular dystrophy (CMD) of varying severity that can affect the brain and eyes, ranging from Walker-Warburg syndrome with severe brain malformation to milder CMD presentations with affected or normal cognition and later onset. Mutations in dystroglycanopathy genes affect a specific glycoepitope on α-dystroglycan (αDG);

Send correspondence and reprint requests to: Carsten G. Bönnemann, MD, National Institute of Neurological Disorders and Stroke/NIH, Porter Neuroscience Research Center, 35 Convent Drive, Bldg. 35, Room 2A-116, Bethesda, MD 20892-3705. Telephone: 301-594-5496; Fax: 301-480-3365; carsten.bonnemann@nih.gov.

of the 14 genes implicated to date, *LARGE* is the glycosyltransferase that adds the final xylose and glucuronic acid, allowing αDG to bind ligands including laminin 211 and neurexin. Only 11 patients with *LARGE* mutations have been reported. We report the clinical, neuroimaging and genetic features of 4 additional patients. We confirm that gross deletions and rearrangements are important mutational mechanisms for *LARGE.* The brain abnormalities overshadowed the initially mild muscle phenotype in all 4 patients. We present the first comprehensive postnatal neuropathology of the brain, spinal cord and eyes of 1 patient with a homozygous *LARGE* mutation at Cys443; in this patient, polymicrogyria was the predominant cortical malformation; densely festooned polymicrogyria were overlaid by a continuous agyric surface. In view of the severity of these abnormalities, Cys443 may be a functionally important residue in the LARGE protein whereas the mutation p.Glu509Lys of Patient 1 in this study may confer a milder phenotype. Overall, these results expand the clinical and genetic spectrum of dystroglycanopathy.

Keywords

Agyria; Congenital muscular dystrophy; Dystroglycanopathy; LARGE; Neuropathology; Polymicrogyria

INTRODUCTION

Congenital muscular dystrophy (CMD) is the second most common form of muscular dystrophy after Duchenne Muscular Dystrophy (1, 2). CMD is comprised of a phenotypically and genetically heterogeneous group of disorders with congenital onset and dystrophic findings on muscle biopsy (3). Dystroglycanopathies, along with collagen 6 and laminin α 2-related forms, are the most common forms of CMD (4-6).

Mutations in several genes that normally modify the function of dystroglycan (primarily through glycosylation of its α subunit) result in dystroglycanopathies (7, 8). Dystroglycan, which is encoded by the single DAG1 gene, undergoes posttranslational processing into β-dystroglycan, which binds to dystrophin and spans the sarcolemma, and α-dystroglycan (αDG), which binds to β-dystroglycan on the extracellular side and acts as an important matrix receptor (9, 10). αDG binds extracellular ligands such as laminin 211 at the sarcolemma, neurexin in the brain, and agrin at the neuromuscular junction; thus, it plays important roles in sarcolemmal and basement membrane stability and neuronal cell migration as well as having other putative functions (1, 10-13). The current understanding of the mechanism(s) behind abnormal neuronal migration is that hypoglycosylation or conditional deletion of αDG interferes with the interaction between αDG and extracellular matrix proteins. The dystrophin-glycoprotein complex likely becomes destabilized on radial glial cells, resulting in the neurons over-migrating and breaching the glia limitans with the final result of disordered lamination of the cerebral cortex and neuronal and glial heterotopias. The basal lamina molecular composition may be affected depending on the subtype of dystroglycanopathy (1, 14).

The binding of the extracellular ligands mentioned above is dependent on a specific glycoepitope of the extracellular α subunit, which is generated in several steps. The first involves a special O-mannosyl glycosylation added by the glycosyltransferases POMT1,

POMT2 and POMGnT1, followed by the addition of a second glycoepitope that is dependent on the addition of a phosphate residue and on the activity of the *LARGE, FKRP* and *FKTN* gene products (15). LARGE (acetylglucosaminyltransferase-like protein, OMIM 603590) was recently shown to have bi-functional glycosyltransferase function, adding a xylose/glucuronic acid repeat unit that is crucially responsible for the binding activity of αDG (16). The precise molecular roles of fukutin-related protein (FKRP) and fukutin (FKTN) are not fully understood and may include chaperone-like as well as glycosyltransferase functions. Recently, *ISPD* has been identified as another gene causing Walker-Warburg syndrome; its exact function is also still unknown but it may facilitate the early, POMT1-dependent glycosylation of αDG (17, 18). Mutations in *GTDC2, B3GNT1, B3GALNT2, TMEM5, GMPPB, and SGK196* also cause dystroglycanopathies (19-23). The functions of these gene products are currently uncharacterized but glycosyltransferase activities are predicted. The crucial role for LARGE in the final addition of the second glycoepitope is reinforced by the observation that overexpression of LARGE is capable of partially rescuing hypoglycosylation as a result of mutations not only in *LARGE* itself but also in *FKRP*, *FKTN* and *POMGnT1* (24-26). The pathological phenotype in dystroglycanopathies is due to lack of the LARGE-dependent glycoepitope that is ultimately responsible for binding αDG ligands in muscle, brain and eye.

In addition to these 11 known or putative glycosyltransferases, which modify glycosylation of αDG (27), a mutation in *DAG1* itself has also been described (28). Although situated in αDG, the mutation in effect also interferes with the proper glycosylation of αDG (28). The *DAG1* mutation has been referred to as a primary dystroglycanopathy while the mutations in the modifying genes have been referred to as secondary dystroglycanopathies (26). Mutations in genes associated with other congenital disorders of glycosylation may also interfere with αDG glycosylation, and in addition, there is evidence for additional as yet undiscovered genes in the pathway (26). Without sufficient post-transcriptional modification, αDG does not bind its extracellular ligands properly, resulting in defects of both neurons and glia attributable to defects in the basement membrane in the muscle and brain; there is also evidence of more subtle defects at the synaptic level (1, 29).

The *LARGE* gene, the fifth largest locus in the human genome (and thus so named [30]), was identified as a causative gene in dystroglycanopathy based on the findings that the naturally occurring myodystrophy mouse model carried a null mutation in *Large* (31). The Large^{myd} mouse phenotype is caused by a 100 KB genomic deletion in its homologous *Large* gene, resulting in loss of the crucial binding αDG glycoepitope with evidence for both a muscular dystrophy as well as evidence for abnormal neuronal migration (31). Because of its strong potential as a candidate gene, Longman et al investigated *LARGE* mutations by linkage and sequencing in 36 patients with muscular dystrophy and either mental retardation, structural brain changes, or abnormal αDG on immunolabelling without a mutation in the known genes at the time. They identified the first patient with a mutation in *LARGE* (32). To date, only 11 patients in 8 families have been reported with mutations in *LARGE* (33, 34).

We report 4 additional *LARGE*-related dystroglycanopathy cases with great variability in clinical presentation, each with novel mutations in *LARGE,* and provide the first postnatal

comprehensive neuropathological evaluation of the brain, spinal cord and eyes in a patient with LARGE deficiency. This evaluation most resembled findings first described in Fukuyama CMD, but with additional findings relating to the nature of polymicrogyria, thick tectum, abnormal fiber tracking in the brainstem, and axonal abnormalities. Further understanding of LARGE is important given its central role in generating the functional glycoepitope on αDG and the unique observation that increasing its activity (with resulting hyper-glycosylation of αDG) has been shown to ameliorate the muscle phenotype of dystroglycanopathies (24, 26), thereby providing potential therapeutic avenues through modulation of LARGE activity.

MATERIALS AND METHODS

Patients

P1 is a 7-year-old female with no relevant family history (Fig. 1A). She was the product of a term pregnancy and was delivered by Cesarean section for failure to progress. She had no signs of hypotonia at birth and was discharged home with her mother. She was first noted to have motor and speech delay by her parents at age 1 year when she did not sit independently, walk or talk.

Her motor milestones were as follows: held head by 3 months, rolled before 3 months, put into sitting position by 6 months, never crawled, stood independently at 2 years, walked at 2 years, and ran at 5 years. At 7 years of age, she currently climbs up stairs alternating feet without holding onto a rail and climbs down stairs one step at a time as needed. She is able to run and rise from the floor. She began talking shortly before 3 years of age and now has a vocabulary of several hundred words. She was first noted to have hypotonia and failure to thrive at age 15 months when her pediatrician referred her to early intervention services. She continues to make significant gains in gross motor development and strength. She can feed herself but cannot write her own name. She completed toilet training at age 6 years. She has no pulmonary, cardiac, hematological, endocrinological or dermatological involvement. Because of the recognition of a brain malformation on magnetic resonance imaging (MRI) and elevated transaminases (before it was clear that they originated from muscle) she was initially suspected of having congenital CMV infection.

P2 was a 9-month-old female born to consanguineous parents (Fig. 1B); the pregnancy was complicated by late prenatal care. A fetal ultrasound suggesting hydrocephalus prompted an MRI, which revealed hydrocephalus with an abnormal gyral pattern. There was bilateral wrist flexion. After 41 weeks gestation the mother was induced and the baby delivered vaginally. She was transferred to the NICU for respiratory support, an abnormal neurologic exam and poor feeding that required placement of a G-tube. A ventriculoperitoneal shunt was placed for the hydrocephalus. She was found to have low bone density 2 months before death when she had a fracture of the femur. Her mother provided constant care because the baby had recurrent pneumonia, was ventilator-dependent, and had gastroesophageal reflux requiring Nissen fundoplication and a G-tube for feeding. She expired at age 9 months of age due to respiratory failure.

P3 is a 3-year-old boy who is the child of parents from the same small town in Venezuela but without known consanguinity (Fig. 1C). There is no family history of neuromuscular disease. He was noted to have hydrocephalus at birth requiring a ventriculoperitoneal shunt. At 2 months of age he was seen by a neurologist for apnea and was noted to have elevated serum creatine kinase and transaminases. He has not shown developmental progress over time and is currently unable to sit, roll over, crawl, babble, or use his hands. He started to have seizures at age 8 months involving staring spells lasting up to 5 minutes as well as generalized stiffening episodes, which may occur in clusters lasting up to 25 minutes. Seizures are currently controlled by valproic acid and phenobarbital. Surgical history includes ventriculoperitoneal shunt at birth, G-tube and Nissen fundoplication at age 2 months, and tracheostomy at age 16 months.

P4 is a 6-month-old infant born to consanguineous parents (1st degree cousins) (Fig. 1D). He was noted to have large ventricles and head circumference in utero. His birth weight was 2975 gm and head circumference was 39 cm. Apgars were 8 and 9 at 1 and 5 minutes. He was admitted to NICU for observation and work up; he was able to feed via a nasogastric tube and had no respiratory issues. His anterior fontanel was flat and measured 3 × 3 cm. He was hypotonic with reduced limb movement and deep tendon reflexes. An ophthalmology consult confirmed bilateral retinal detachment and follow-up revealed blindness with severe developmental delay but no seizures. At age of 4 months he developed signs of increased intracranial pressure and a ventriculoperitoneal shunt was inserted.

Genotyping

In P1, single nucleotide polymorphism (SNP) array was performed using Illumina HumanQuad610 BeadChip on DNA prepared from peripheral blood. Amplification and sequencing of the full coding regions and approximately 50 bases of flanking sequence of *LARGE* exons was performed using genomic DNA extracted from the patient's blood. In P2, amplification and sequencing of coding regions for all 7 dystroglycanopathy genes were performed using genomic DNA obtained from blood. In P3, in addition to amplification and sequencing as described above, Array Comparative Genomic Hybridization analysis using custom designed oligo-array containing 44,000 oligos (Agilent Technologies, Palo Alto, CA) was used. Custom designed, oligo-based array comparative genomic hybridization microarray for *LARGE* (Prevention Genetics, Marshfield, WI) was used for P3 and P4.

Brain MRI

3 Tesla brain MRIs (P1) and 1.5 Tesla brain MRIs (P2-P4) were performed and T1, T2, and T2 FLAIR axial and sagittal images were acquired.

Postmortem Studies of Brain, Spinal Cord and Eyes of P2

Postmortem tissue was fixed in formaldehyde and processed through paraffin. Stains utilized for evaluation included hematoxylin and eosin (H&E), Trichrome, Bodian and Klüver-Barrera stains. Immunohistochemistry was performed routinely by immunoperoxidase using antibodies to epithelial membrane antigen, neurofilament protein, neuronal nuclei, and glial fibrillary acidic protein. Cerebral cortical laminar organization was assessed with antibodies to the following: reelin (MAB5366, Chemicon, Temecula, CA), special AT-rich sequence-

binding protein 2 (SATB2, Bio Matrix Research, Iwai North America, Foster City, CA), chicken ovalbumin upstream promoter transcription factor-interacting protein 2(cTip2, ab18465, Abcam, Cambridge, MA), and anti-transcription factor T-Box, brain, 1 (TBR1) (kindly provided by Dr. Robert Hevner, University of Washington, Seattle, WA). All procedures were performed as previously described (35).

Muscle Biopsies

Skeletal muscle from the left thigh of P1 was biopsied, frozen, and stained with standard H&E, modified Gomori trichrome, periodic acid Schiff, picrosirius, Oil-Red-O, enzyme histochemical methods, NADH-TR, ATPase at pH 9.4 and pH 4.3, succinic acid dehydrogenase (SDH), cytochrome oxidase (COX), combined SDH-COX, and immunohistochemistry for fast, slow, and neonatal myosins and HLA class I.

Rectus abdominis muscle of P3 was biopsied. Two slides each were stained with H&E, Trichrome, SDH, COX, periodic acid Schiff, Oil Red O, developmental myosin, and 6 slides were stained for myosin ATPase, 1 for Merosin (Merosin-N: Abcam (ab11576), 1 for Merosin-C: (Novocastra, Leica, Buffalo Grove, IL) (Merosin-CE), 1 for αDG (Abcam (ab106110)), and for 1 Collagen VI.

Immunofluorescence on Muscle Biopsy of P1

Skeletal muscle sections, 9 μm thick, were fixed in 100% methanol and washed twice in 1X phosphate-buffered saline. Sections were blocked in 0.1% Tx-100/10% fetal bovine serum/ phosphate-buffered saline at room temperature for 1 hour and then incubated with primary antibodies (anti-VIA4-1, a gift from Kevin Campbell diluted at 1:20) overnight at 4°C. AlexaFluor secondary antibodies (goat anti-mouse568 1:500 + goat anti-rabbit488 1:500) were used followed by mounting with Fluoromount-G. Images were acquired on a Nikon epi-fluorescent microscope.

Immunoblotting on Muscle Biopsy of P1

Antibodies to a-dystroglycan (IIH6 and VIA4-1, gifts from Kevin Campbell at 1:50) were used. Proteins were resolved by electrophoresis on a 4%-12% gradient Bis-Tris polyacrylamide gel and blotted according to a standard protocol. Goat anti-mouse IgG conjugated to horseradish peroxidase was used as a second antibody. The blot was developed with ECL Western blotting detection reagents (GE Healthcare, Little Chalfont, Buckinghamshire, UK), according to the manufacturer's instructions.

Neurocognitive Testing of P1

Neurocognitive testing was performed by a board-licensed neuropsychologist. Tests were administered in a secluded room with the mother present and included the Wechsler Nonverbal Scale of Ability, the Peabody Picture Vocabulary Test-4, and the WPPSI-III Naming Subtest. Two parent scales were also administered to the patient's mother: the Child Behavior Check List and the Vineland Adaptive Behavior Scales—II.

Muscle Ultrasound on P1

Standard medical soft tissue ultrasound of the muscles was performed using a Siemens S2000 system. An 18L6 HD transducer was used at 15 MHz to examine the lower extremity muscles (vastus lateralis and medialis, rectus femoris, hamstrings, soleus, medial and lateral gastrocnemii), and upper extremity muscles (anterior and posterior deltoid, biceps, and triceps).

RESULTS

Neurological Examination

A summary of the results of neurological exams of the 4 patients is shown in Table 1. For P1, the timed functional test results at age 7 years were as follows: stand from supine, score 5, time 2.7 seconds; 10 m run, score 6, time 4.8 seconds; ascend stairs, score 6, time 3.1 seconds; descend stairs, score 5, time 6.0 seconds.

Creatine Kinase Levels

Creatine kinase levels were markedly elevated in all patients (Table 2).

Genetic Testing

Genetic testing for P1 revealed recessively inherited compound heterozygous mutations in *LARGE*, including a not-yet reported 74-kb deletion (Chr22:32330175-32403758, Human Genome Build 36) containing part of *LARGE* gene initially identified by SNP analysis (paternally inherited), followed by identification of a previously reported missense mutation on the other allele p.Glu509Lys (c.1525G>A) (32) by sequencing (maternally inherited).

For P2, sequencing of all 7 dystroglycanopathy genes (initiated because of the suggestive MRI findings) revealed a novel homozygous 2 base pair deletion/insertion variant in *LARGE* consistent with the history of consanguinity, c.1328_1329delGCinsAT (p.Cys443Tyr). P3 initially received an abnormal microarray comparative genomic hybridization result that included a deletion in *LARGE.* DNA sequencing of dystroglycan related CMD genes resulted in an inconclusive finding in *LARGE*: exon 7 did not amplify despite repeated attempts. Further genetic testing using a higher resolution microarray containing probes of *LARGE* revealed 2 novel deletions: a deletion of exon 7 with breakpoint in intron 6 and intron 7 (c.675+18,311_787+52,924del74,200) and a deletion of exons 3 - 7 with breakpoints in intron 2 and intron 7 (c.1-33,247_787+101,071del330, 947).

Sequencing for P4 was also suggestive of a deletion because PCR amplification from genomic DNA of exons 4, 5, 6, and 7 failed. Subsequent array comparative genomic hybridization testing revealed a novel homozygous deletion of approximately 108 kb in *LARGE.* This deletion encompasses exon 4 to exon 7 with approximate genomic locations chr22:33,959,101 (hg19) in intron 7 and chr22:34,067,070 (hg19) in intron 3. These 5 novel mutations are depicted in Figure 2 in the context of the other *LARGE* mutations identified to date.

Brain MRI

Brain MRI in P1 showed a complex brain malformation with pachygyria/polymicrogyria in a mostly frontoparietal distribution, patchy white matter signal abnormalities in higher parietal white matter on T2/FLAIR images, slightly small pons, but no cerebellar cysts (Fig. 3A-C).

P2's MRI was of suboptimal quality but showed hydrocephalus, absent septum pellucidum, smooth cortical surface in particular of the temporal lobes and the occipital lobes with shallow gyration of the frontal and dorsal brain surface, very small pons and atrophic cerebellum with cerebellar cysts, initially interpreted as consistent with Walker-Warburg syndrome (Fig. 3D-F).

P3's MRI findings included white matter hypo-intensities on T1 frontally and temporally, widespread pachygyria/polymicrogyria frontally and posteriorly, small pons, thick tectum, abnormal cerebellum, absent corpus callosum, and a band-like heterotopic layer in the occipital region (Fig. 3G-I).

P4's brain MRI showed hydrocephalus, disrupted corpus callosum, cystic outpouching of the cerebral mantle, frontal pachygyria/polymicrogyria and temporal lissencephaly/ polymicrogyria, hypoplastic pons, thick tectum, and markedly hypo- and possibly also dysplastic cerebellum. The left eye was dysplastic involving lens and vitreous (Fig. 3J-L).

Postmortem Findings in P2

General postmortem findings included a healthy-appearing, well cared for infant weighing 8790 g (19 lb 6 oz), measuring 71 cm in length (28 inches) with a head circumference 47.5 cm (expected 45 cm). Muscle mass was overall reduced and the extremities were without contractures.

Gross Neuropathological Findings in P2

The brain and spinal cord weighed 741 g (expected brain weight 820 g). The cerebral hemispheres were symmetric but the surface exhibited an abnormal gyral pattern with an irregular surface of the frontal, parietal and occipital lobes, while there was a mostly smooth, agyric pattern of the temporal lobes (Fig. 4A-C). The cerebellum and brainstem were mildly hypoplastic; the cerebellar folia were poorly defined resulting in a partially smooth surface appearance of the cerebellar hemispheres. The optic nerves, chiasm and third nerves were thin but white.

Coronal sections of the cerebral hemispheres disclosed a shallow longitudinal fissure, 2 small supra-callosal gyri, a thin corpus callosum, absence of the septum pellucidum, dilated lateral ventricles and mildly dilated third ventricle. The sulci of the frontal, parietal and occipital lobes were of variable depth whereas they were essentially absent in temporal lobes. The centrum ovale volume was reduced but had the white appearance of normal myelination. The thalamus, basal ganglia and internal capsule were grossly normal (Fig. 4C).

The hypoplastic brainstem showed general attenuation of architecture, but there was no apparent aqueduct; there was a “molar tooth”-like configuration of the 4th ventricle similar to the findings in Joubert syndrome (36). Midbrain tectum appeared thicker than normal. In the pons there was severe hypoplasia of the basis pontis with a mild midline cleft and hypoplastic middle cerebellar peduncles (Fig. 4D). In the medulla oblongata, the olivary bulge was not seen and the pyramids were poorly defined. The cerebellar hemispheric tissue was firm and the folia widened and indistinct. The vermian folia appeared normal and the dentate nuclei were present. The spinal cord was smaller than normal and had a “sombrero hat” configuration, indicative of degeneration or absence of the corticospinal tracts.

Microscopic Neuropathological Findings in P2

The cerebral cortex and white matter of the frontal, parietal, and occipital lobes contained large numbers of neurons, primarily pyramidal, arranged in a festooned pattern (Fig. 5A, B). Sulcal markings were shallow. Focal meningeal fibrosis with obliteration of subarachnoid space, subpial gliosis and occasional herniation of glial tissue into fibrotic meninges were seen. Layer 1 contained large, abnormal neurons. The remaining cortical layers were disorganized (Fig. 5C). These abnormalities were highlighted with neurofilament protein immunohistochemistry and neuronal nuclei stain. The Bodian silver stain indicated the presence of tiny delicate axons that appeared randomly dispersed within cortex and white matter (Fig. 5D). Axons were severely depleted in the temporal lobes. Immunohistochemistry using the anti-Reelin, anti-SATB2, anti-cTip2, and anti-TBR1 antibodies disclosed that neurons of all cortical layers were present but abnormally located.

Although the temporal lobe appeared grossly agyric with a mostly smooth surface, the cortical dysplasia microscopically resembled the typical festooned pattern of polymicrogyria without any evident sulcation. Evaluation of cortical lamination demonstrated both temporal and non-temporal lobe cortices to be disorganized (Table 3). The hippocampus was hypoplastic and characterized by a jumbled arrangement of pyramidal cells and few dentate layer neurons. The thalamus and other deep grey nuclei were partially recognizable, the former less well than the latter. Thalamic nuclei were not recognizable as such although a generous neuronal population was present. The subthalamic nucleus was small; medial and lateral segments of the pallidum were poorly separated. There were scattered dysplastic fiber bundles.

In the cerebellum, the vermian cortex, white matter and dentate nuclei were essentially normal but there was severe dysplasia of the hemispheres. The grey matter consisted of disrupted masses of external and internal granular cells and Purkinje cells with little or no associated white matter (Fig. 6A).

The medulla had a globular configuration. Pyramids were absent but well-formed inferior olivary nuclei and myelin were present (Fig. 6B). The severely hypoplastic pons had essentially no descending cortical tracts, basal neurons, crossing fibers or middle cerebellar peduncles. The midbrain showed excessive tectal volume and aberrant large bundles of myelinated fibers on each side (Fig. 6C). Cranial nerve nuclei in the pontine tegmentum and third nerve in the midbrain contained a minimal number of neurons. The aqueduct was hypoplastic. Extraneous fiber bundles were present in the tectum, which was filled with

large numbers of neurons. All levels of brainstem displayed subpial gliosis with intermixed collagen, most severe in the midbrain where neural tissue had also herniated into the subarachnoid space.

Spinal cord structure was generally preserved, but it had a “sombrero hat” configuration consequent to absence of lateral cortical spinal tracts and an overall paucity of axons. There was striking pial fibrosis containing collagen that formed dense adhesions; these destroyed the pia mater and were continuous with peripheral spinal cord white matter (Fig. 7). Examination of the eyes showed atrophy of retinal ganglion cells and mild secondary gliosis. The optic nerve contained few axons.

Muscle Biopsies

A biopsy of the quadriceps muscle in P1 disclosed mild changes with mild variability in fiber diameter and occasional degenerating and regenerating fibers but no apparent fibrosis, consistent with early dystrophic changes (Fig. 8A). There was a marked reduction of glycosylated αDG on immunostaining in comparison to a normal control sample (Fig. 8B, C), and partially reduced β-dystroglycan and dystrophin II (data not shown). Laminin α2, and α-, β-, and γ-sarcoglycan immunohistochemistry were normal (data not shown). A Western blot demonstrated a reduction in the amount and molecular weight of glycosylated αDG (Fig. 8D). Skeletal muscle from the autopsy on P2 was fixed in formalin and displayed no abnormality on H&E stain.

Muscle biopsy in P3 showed a dystrophic process with fatty replacement. There was perimysial and endomysial fibrosis, fiber size variability due to atrophy and some hypertrophy, small clusters of regenerative fibers with basophilic sarcoplasm, and fiber splitting. Immunohistochemistry showed a complete absence of glycosylated αDG and partial deficiency of merosin (not shown).

Muscle Ultrasound on P1

Muscle ultrasound revealed very mild involvement of the hamstring muscles with a mildly increased, diffuse echogenic signal (Supplemental Fig. 1A). The following muscle groups had normal-appearing echo: rectus femoris (Supplemental Fig. 1.B), gastrocnemii, soleus, deltoid, biceps, and triceps.

Neurocognitive Testing on P1

Results of the Wechsler Nonverbal Scale of Ability, Peabody Picture Vocabulary Test-4, WPPSI-III Naming Subtest, Child Behavior Check List and Vineland Adaptive Behavior Scales—II are shown in Table 4. Based on these results, her adaptive abilities are better developed than reasoning, processing speed, and memory. Her receptive and expressive language skills are equivalent on the Vineland.

DISCUSSION

Prior to this report, 11 children from 8 families with *LARGE* mutations were known. The phenotypes of these patients range from severe Walker-Warburg syndrome to a brain and

muscle phenotype more reminiscent of the Fukuyama/muscle eye brain disease part of the spectrum (27, 32, 37-41). All patients had cognitive delays, elevated creatine kinase when reported, and various MRI findings (Table 2).

We report 4 additional patients with novel mutations and describe the first detailed postnatal neuropathologic study of dystroglycanopathy due to mutations in *LARGE* thereby providing additional characterization of the clinical and genetic spectrum of dystroglycanopathy. To date, all mutations in *LARGE* have been associated with brain involvement and substantial mental retardation, covering a spectrum from Walker-Warburg syndrome to Fukuyama-like changes. Previously reported patients have had various degrees of delayed motor and cognitive milestones. On the less severe end of the spectrum, patients with *LARGE* mutations have been able to achieve walking (32) and climbing stairs while holding a handrail (27). Patients have not been able to run and speech has been reported to be dysarthric (27). MRI findings in previously reported patients include pontine and cerebellar hypoplasia, pontine clefts, cerebellar cysts, lissencephaly, pachygyria, polymicrogyria, dilated ventricles, and abnormal high white matter signal (Table 2).

The clinical severity in our 4 patients also varied greatly but each of them had the same 3 key findings of cognitive delay, elevated creatine kinase, and brain MRI abnormalities. The combination of these 3 major manifestations led to genetic testing for dystroglycanopathy in P2-P4. In the more mildly affected patient, P1, the initial abnormal SNP array identified the mutation in *LARGE*. Despite the brain MRI of P1 showing frontoparietal abnormalities of a thick cortex and broad-appearing gyration consistent with a cortical malformation, mild pontine hypoplasia, and patchy white matter hyper-intensities, her clinical findings were surprisingly moderate, including a vocabulary of several hundred words and the ability to walk, run, climb stairs, and use the toilet. On the other hand, P2-P4 had more widespread brain malformations and much more severe clinical findings with profound early weakness, ophthalmologic involvement, hypotonia, and developmental delay.

LARGE consists of a transmembrane domain, a coiled-coiled domain, and 2 catalytic domains, consistent with its recently confirmed dual glycosyltransferase activity, adding a repeat xylose-glucuronic acid disaccharide unit as the LARGE-dependent glycoepitope (16). The gross deletions in P1, P3, and P4 span exons 4-7 of *LARGE*, including the C terminal end of the first catalytic domain, resulting in a predicted complete loss of function of that allele. Given that P1 was comparatively milder to the others, we speculate that the previously reported c.1525G>A missense mutation, her second mutation, is responsible for ameliorating the phenotype. The previously reported case with this missense mutation likewise had a relatively milder (muscle eye brain disease) phenotype and is the only other patient to date (like P1) to achieve walking (32). In contrast, in view of the clinical and pathological severity of the second patient, her homozygous deletion-insertion c. 1328_1329delGCinsAT resulting in the amino acid change p.Cys443Tyr suggests this residue plays a functionally important role in the LARGE protein; however, its exact function within the still evolving understanding of LARGE structure-function relationships remains to be clarified. Although the p.Cys443 amino acid lies outside of either of the 2 glycosyltransferase domains, its importance to the function of LARGE is supported by its complete conservation through evolution (conserved from human to *C. elegans*). Deletions

and rearrangements such as those in P1 and P4 have been previously reported in *LARGE*. To our knowledge, however, our patient P3 is the first case in which 2 different gross deletions have been found in the same patient. Because gross deletions and rearrangements of *LARGE* represent an important class of mutations, and because they may be missed by direct sequencing, such mutations should be excluded in the diagnostic process using microarray, reverse transcriptase PCR, or other appropriate quantitative methodologies (41).

Finally, we provide the first description of post-natal neuropathological findings of the brain and spinal cord in a patient with a confirmed *LARGE* mutation. Analysis of the brain and spinal cord of P2 revealed findings that are most closely related to the pathology described in Fukuyama CMD and muscle eye brain disease, as well as a fetal population with *LARGE* mutations (38, 42-44), with some notable differences. The abnormal cortical surface in the dystroglycanopathies ranges from coarse and granular to almost smooth (45). For the smooth areas historically, the term “cobblestone lissencephaly” (corresponding to lissencephaly type II) (46, 47) was introduced to distinguish this unique malformation from classical 4-layer lissencephaly (corresponding to lissencephaly type I) and to reflect the still rough or bumpy-appearing surface when compared to classical 4-layer lissencephaly. The typical histological finding in “cobblestone lissencephaly” is an extensive abnormal layer of over-migrated neurons beyond the glia limitans of the brain. This type of complete lissencephalic malformation was not prominent histologically in our patient. Rather, we noted variable degrees of polymicrogyria, which was densely folded and was overlaid by a fused layer of neurons that had over-migrated into the subarachnoid space; this was most conspicuous over the temporal lobes where an agyric cortical surface was apparent. Thus, polymicrogyria with neuronal over-migration of varying degrees was the universal cortical finding and resulted in different cortical surface appearances from irregular gyration to agyric. This spectrum may be difficult to delineate fully on in-vivo imaging. It is of interest that in the extensive fetal series of dystroglycanopathy brains, all 3 cases with *LARGE* mutations were described as being of intermediate severity (cobblestone lissencephaly type B in their classification), with the residual cortical plate showing polymicrogyria (43), consistent with the findings we report here. Thus, these findings appear to be quite unique among cerebral changes reported in association with dystroglycanopathies and may be used to guide molecular screening directly toward *LARGE* (43).

We also observed a markedly disorganized cerebellum and abnormal fiber tracking in the brainstem, indicating that αDG is also involved in infratentorial neuronal path-finding and confirming similar findings in the prenatal series (43). Another striking finding in the brainstem was the thick tectum that appears to have a higher neuronal density as the basis for this enlargement. A thick tectum is a frequent and useful finding on MRI of patients with dystroglycanopathy (38). In a careful examination of brainstem findings in patients with Fukuyama CMD, a thick tectum has been noted with evidence of overlying glioneuronal heterotopias but no mention of neuronal cell content (42). Interestingly, however, increased neuron content of the tectum has been mentioned in a chick model of αDG dysfunction (48) and more closely resembles the observation in our patient. There was no specific mention of the tectum in the fetal series of dystroglycanopathy brains (43).

There are several other aspects of the pathology of P2 that deserve comment. Perhaps the most intriguing are the axonal abnormalities. In spite of the large numbers of neurons in the cortex, axons were delicate, fragmented and randomly distributed in white matter. This would help account for agenesis of the corticospinal tracts but at the same time does not explain the dislocated bundles of myelinated fibers in deep cerebrum that are of obscure origin. This finding may suggest a profound disturbance in axonal integrity. The second issue involves herniation of cerebral tissue into the subarachnoid space as a result of the over-migration that we addressed in our earlier discussion of the polymicrogyria. This was comparatively minimal in the supratentorial brain of P2 but was striking in the ventral border of the spinal cord, and, furthermore, associated with marked meningeal fibrosis. Finally, there were no developmental abnormalities of the eyes except for loss of retinal ganglion cells and axons in the optic nerves.

Overexpression of LARGE, not only in mice with *LARGE* mutations but also in mice with mutations in POMGnT1 and FKTN, restores some of the crucial glycoepitope of α-dystroglycan. Thus, binding of its extracellular ligands is rescued in cell culture and in muscle, thereby ameliorating the phenotype in mice. While amelioration of the cortical migration defect is unlikely, it is possible that synaptic or other CNS connectivity defects might be improved. Further understanding of the function of LARGE and the role of these mutations is critical in view of its crucial position in the glycosylation pathway of αDG and its potential therapeutic benefit for some aspects of α dystroglycanopathies when it is upregulated.

Supplementary Material

Refer to Web version on PubMed Central for supplementary material.

ACKNOWLEDGMENTS

The authors thank the patients and their families for their participation in this case study. We also gratefully acknowledge Dr. Russell Butterfield for assistance with the human *LARGE* domain structure, Dr. Edythe Wiggs for her expertise with the neurocognitive testing, Ms. Rachel Mascareno for her work with the neuropathology staining, and Ms. Elizabeth Hartnett for organization of P1's visits to NIH.

Katherine G. Meilleur, Kristen Zukosky, **ND????**, Ying Hu, Sandra Donkervoort and Carsten G. Bönnemann received funding from the intramural NINDS for this study.

REFERENCES

1. Michele DE, Barresi R, Kanagawa M, et al. Post-translational disruption of dystroglycan-ligand interactions in congenital muscular dystrophies. Nature. 2002; 418:417–22. [PubMed: 12140558]
2. Muntoni F, Brockington M, Torelli S, et al. Defective glycosylation in congenital muscular dystrophies. Curr Opin Neurol. 2004; 17:205–9. [PubMed: 15021250]
3. Emery AE. The muscular dystrophies. Lancet. 2002; 359:687–95. [PubMed: 11879882]
4. Matsumoto H, Hayashi YK, Kim DS, et al. Congenital muscular dystrophy with glycosylation defects of α-dystroglycan in Japan. Neuromusc Disord. 2005; 15:342–48. [PubMed: 15833426]
5. Peat RA, Smith JM, Compton AG, et al. Diagnosis and etiology of congenital muscular dystrophy. Neurol. 2008; 71:312–21.

6. Clement EM, Feng L, Mein R, et al. Relative frequency of congenital muscular dystrophy subtypes: analysis of the UK diagnostic service 2001-2008. Neuromusc Disord. 2012; 22:522–7. [PubMed: 22480491]
7. Moore SA, Winder SJ. The inside and out of dystroglycan post-translational modification. Neuromusc Disord. 2012; 22:959–65. [PubMed: 22770978]
8. Jae LT, Raaben M, Riemersma M, et al. Deciphering the glycosylome of dystroglycanopathies using haploid screens for Lassa virus entry. Science. 2013; 340:479–83. [PubMed: 23519211]
9. Ervasti JM, Campbell KP. Membrane organization of the dystrophin-glycoprotein complex. Cell. 1991; 66:1121–31. [PubMed: 1913804]
10. Martin PT. Dystroglycan glycosylation and its role in matrix binding in skeletal muscle. Glycobiology. 2003; 13:55R–66R.
11. Ibraghimov-Beskrovnaya O, Ervasti JM, Leveille CJ, et al. Primary structure of dystrophin-associated glycoproteins linking dystrophin to the extracellular matrix. Nature. 1992; 355:696–702. [PubMed: 1741056]
12. Herbst R, Iskratsch T, Unger E, et al. Aberrant development of neuromuscular junctions in glycosylation-defective Large(myd) mice. Neuromusc Disord. 2009; 19:366–78. [PubMed: 19346129]
13. Yoshida-Moriguchi T, Liping Yu L, Stalnaker SH, et al. *O*-Mannosyl phosphorylation of α-dystroglycan is required for laminin binding. Science. 2010; 327:88–92. [PubMed: 20044576]
14. Waite A, Brown SC, Blake D. The dystrophin-glycoprotein complex in brain development and disease. Trends Neurosci. 2012; 35:487–96. [PubMed: 22626542]
15. Barresi R, Campbell KP. Dystroglycan: from biosynthesis to pathogenesis of human disease. J Cell Sci. 2006; 119:199–207. [PubMed: 16410545]
16. Inamori K, Yoshida-Moriguchi T, Hara Y, et al. Dystroglycan function requires xylosyl- and glucuronyltransferase activities of LARGE. Science. 2012; 335:93–6. [PubMed: 22223806]
17. Roscioli T, Kamsteeg EJ, Buysse K, et al. Mutations in ISPD cause Walker-Warburg syndrome and defective glycosylation of α-dystroglycan. Nat Genet. 2012; 44:581–5. [PubMed: 22522421]
18. Willer T, Lee H, Lommel M, et al. *ISPED* loss-of-function mutations disrupt dystroglycanO-mannosylation and cause Walker-Warburg syndrome. Nat Genet. 2012; 44:575–80. [PubMed: 22522420]
19. Manzani MC, Tambunan DE, Hill RS, et al. Exome sequencing and functional validation in zebrafish identify GTDC2 mutations as a cause of Walker-Warburg Syndrome. Am J Hum Genet. 2012; 91:541–7. [PubMed: 22958903]
20. Buysse K, Riemersma M, Powell G, et al. Missense mutations in β-1,3-N-acetylglucosaminyltransferase 1 (B3GNT1) cause Walker-Warburg syndrome. Hum Mol Genet. 2013; 22:1746–54. [PubMed: 23359570]
21. Stevens E, Carss KJ, Cirak S, et al. Mutations in B3GALNT2 cause congenital muscular dystrophy and hypoglycosylation of α-dystroglycan. Am J Hum Genet. 2013; 92:354–65. [PubMed: 23453667]
22. Vuillaumier-Barrot S, Bouchet-Séraphin C, Chelbi M, et al. Identification of mutations in TMEM5 and ISPD as a cause of severe cobblestone lissencephaly. Am J Hum Genet. 2012; 91:1135–43. [PubMed: 23217329]
23. Carss KJ, Stevens E, Foley AR, et al. Mutations in GDP-mannose pyrophosphorylase B cause congenital and limb-girdle muscular dystrophies associated with hypoglycosylation of α-dystroglycan. Am J Hum Genet. Jul 11.2013 93:29–41. [PubMed: 23768512]
24. Barresi R, Michele DE, Kanagawa M, et al. LARGE can functionally bypass α-dystroglycan glycosylation defects in distinct congenital muscular dystrophies. Nat Med. 2004; 10:696–703. [PubMed: 15184894]
25. Kanagawa M, Nishimoto A, Chivonobu T, et al. Residual laminin-binding activity and enhanced dystroglycan glycosylation by LARGE in novel model mice to dystroglycanopathy. Hum Mol Genet. 2009; 18:621–31. [PubMed: 19017726]
26. Brockington M, Torelli S, Sharp PS, et al. Transgenic overexpression of LARGE induces a-dystroglycan hyperglycosylation in skeletal and cardiac muscle. PLoS One. 2010; 5:e14434. [PubMed: 21203384]

27. Clarke NF, Maugenre S, Vandebrouck A, et al. Congenital muscular dystrophy type 1D (MDC1D) due to a large intragenic insertion/deletion, involving intron 10 of the *LARGE* gene. Eur J Hum Genet. 2011; 19:452–7. [PubMed: 21248746]
28. Hara Y, Balci-Hayta B, Yoshida-Moriguchi T, et al. A dystroglycan mutation associated with limb-girdle muscular dystrophy. N Engl J Med. 2011; 364:939–46. [PubMed: 21388311]
29. Moore SA, Saito F, Chen J, et al. Deletion of brain dystroglycan recapitulates aspects of congenital muscular dystrophy. Nature. 2002; 418:422–5. [PubMed: 12140559]
30. Peyrard M, Seroussi E, Sandberg-Nordqvist AC, et al. The human *LARGE* gene from 22q12.3-q13.1 is a new, distinct member of the glycosyltransferase gene family. Proc Natl Acad Sci U S A. 1999; 96:598–603. [PubMed: 9892679]
31. Grewal PK, Holzfeind PJ, Bittner RE, et al. Mutant glycosyltransferase and altered glycosylation of αDG in the myodystrophy mouse. Nat Genet. 2001; 28:151–4. [PubMed: 11381262]
32. Longman C, Brockington M, Torelli S, et al. Mutations in the human *LARGE* gene cause MDC1D, a novel form of congenital muscular dystrophy with severe mental retardation and abnormal glycosylation of αDG. Hum Mol Genet. 2003; 12:2853–61. [PubMed: 12966029]
33. Online Mendelian Inheritance in Man, OMIM®.. Johns Hopkins University; Baltimore, MD: MIM Number: {#613154}: {2/24/2011}:. World Wide Web URL: http://omim.org/
34. Online Mendelian Inheritance in Man, OMIM®.. Johns Hopkins University; Baltimore, MD: MIM Number: {#608840}: {9/15/2011}:. World Wide Web URL: http://omim.org/
35. Judkins AR, Martinez D, Ferreira, et al. Polymicrogyria includes fusion of the molecular layer and decreased neuronal populations, but normal cortical laminar organization. J Neuropathol Exp Neurol. 2011; 70:438–43. [PubMed: 21572338]
36. Sarikaya B, Akpina E, Karli-Oguz K, et al. Joubert syndrome: magnetic resonance imaging findings. Neuroanat. 2004; 3:30–31.
37. Godfrey C, Clement E, Mein R, et al. Refining genotype-phenotype correlations in muscular dystrophies with defective glycosylation of dystroglycan. Brain. 2007; 130:2725–35. [PubMed: 17878207]
38. Clement E, Mercuri E, Godfrey C, et al. Brain involvement in muscular dystrophies with defective dystroglycan glycosylation. Ann Neurol. 2008; 64:573–82. [PubMed: 19067344]
39. van Reeuwijk J, Grewal PK, Salih MA, et al. Intragenic deletion in the *LARGE* gene causes Walker-Warburg syndrome. Hum Genet. 2007; 121:685–90. [PubMed: 17436019]
40. Mercuri E, Messina S, Bruno C, et al. Congenital muscular dystrophies with defective glycosylation of dystroglycan: a population study. Neurol. 2009; 72:1802–9.
41. Vuillaumier-Barrot S, Bouchet-Seraphin C, Chelbi M, et al. Intragenic rearrangements in *LARGE* and *POMGNT1* genes in severe dystroglycanopathies. Neuromusc Disord. 2011; 21:782–90. [PubMed: 21727005]
42. Saito Y, Kobayashi M, Itoh M, et al. Aberrant neuronal migration in the brainstem of Fukuyama-type congenital muscular dystrophy. J Neuropathol Exp Neurol. 2003; 62:497–508. [PubMed: 12769189]
43. Devisme L, Bouchet C, Gonzales M, et al. Cobblestone lissencephaly: neuropathological subtypes and correlations with genes of dystroglycanopathies. Brain. 2012; 135:469–82. [PubMed: 22323514]
44. Jissendi-Tchofo P, Kara S, Barkovich AJ. Midbrain-hindbrain involvement in lissencephalies. Neurol. 2009; 72:410–8.
45. Takada K, Nakamura H, Tanaka J. Cortical dysplasia in congenital muscular dystrophy with central nervous system involvement (Fukuyama type). J Neuropathol Exp Neurol. 1984; 43:395–407. [PubMed: 6737009]
46. Forman MS, Squier W, Dobyns WB, et al. Genotypically defined lissencephalies show distinct pathologies. J Neuropathol Exp Neurol. 2005; 64:847–857. [PubMed: 16215456]
47. Barkovich AJ, Kuzniecky RI, Jackson GD, et al. Classification system for malformations of cortical development: update 2001. Neurology. 2001; 57:2168–78. [PubMed: 11785496]
48. Schröder JE, Tegeler MR, GroBhans U, et al. Dystroglycan regulates structure, proliferation and differentiation of neuroepithelial cells in the developing vertebrate CNS. Develop Biol. 2007; 307:62–78. [PubMed: 17512925]

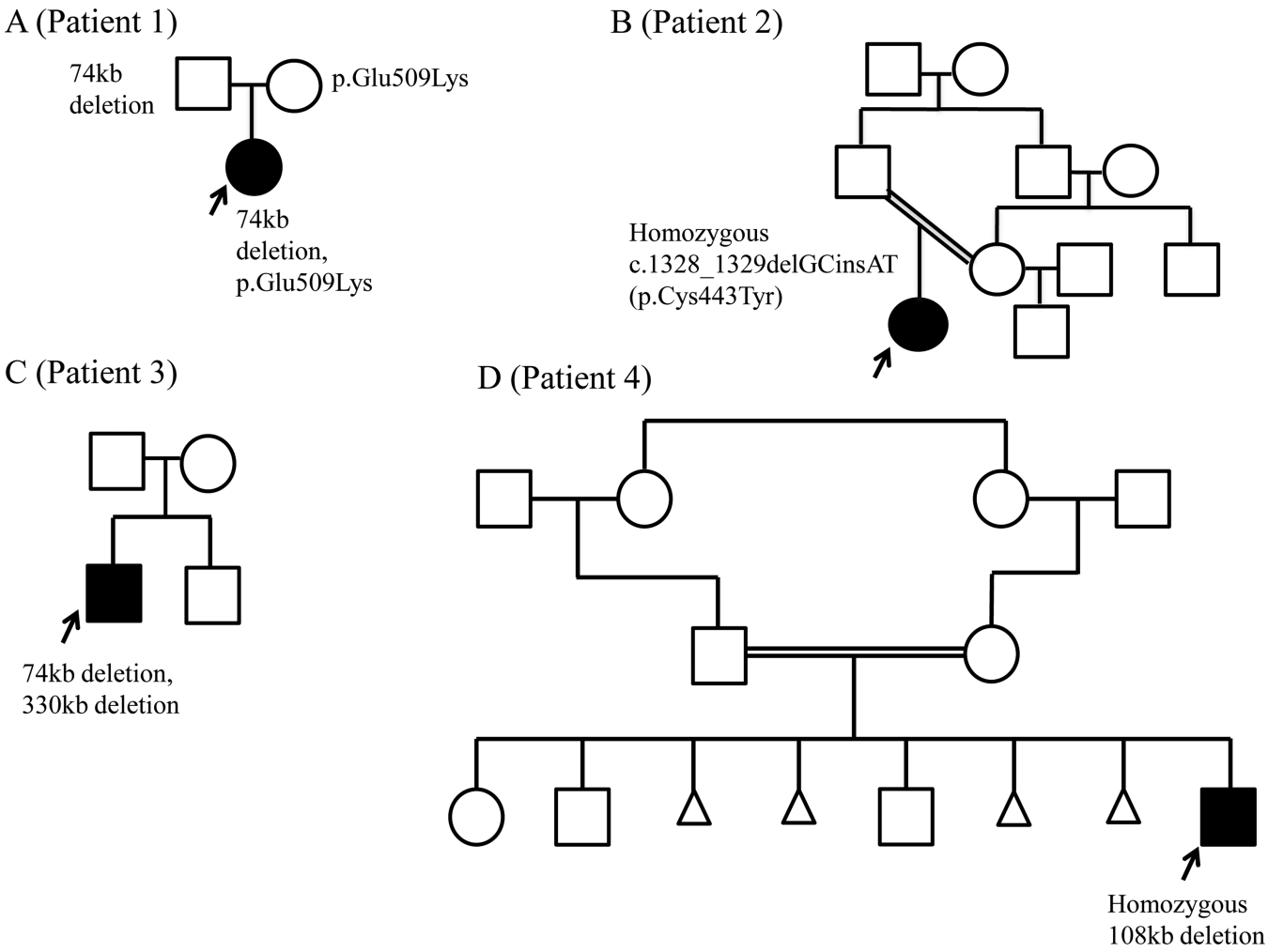

Figure 1.
Family pedigrees of patients (P1-P4). (**A**) P1; (**B**) P2; (**C**) P3; (**D**) P4.

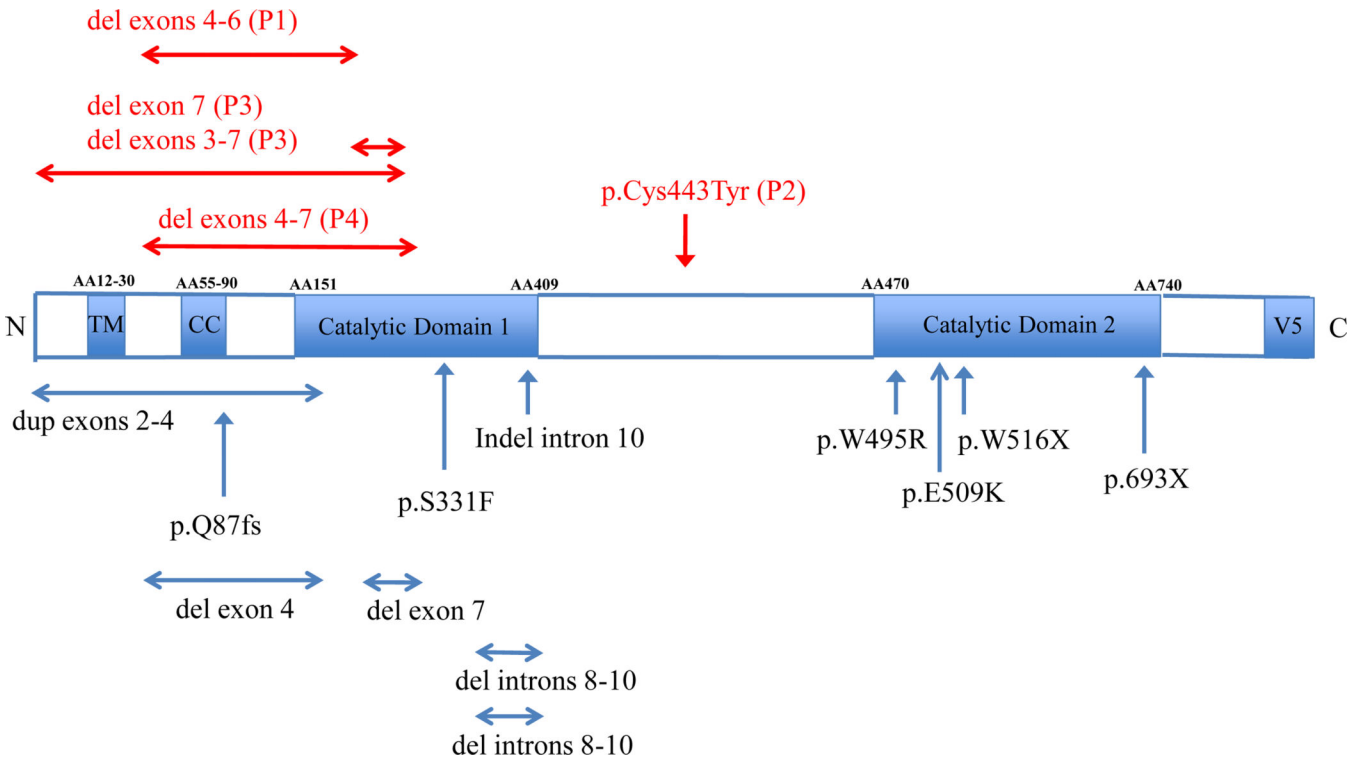

Figure 2.

Domain structure and location of LARGE mutations identified to date. AA = amino acid; N = N terminal; C = C terminal; TM = transmembrane domain; CC = coiled-coiled domain; V5 = expression vector; mutations in red are novel (this report).

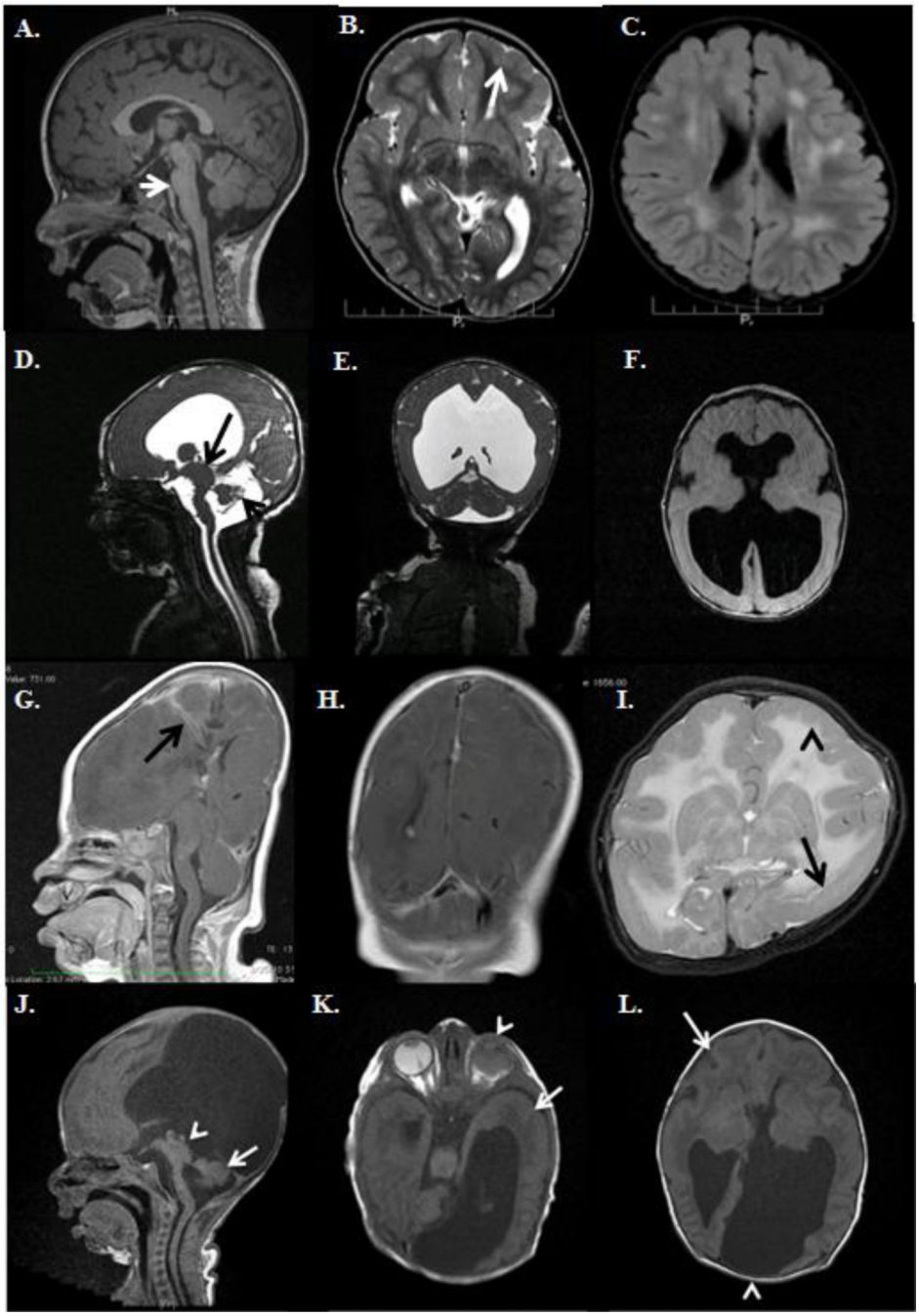

Figure 3.

Brain magnetic resonance imaging of patients P1-P4. (**A-C**) P1. Sagittal T1 image shows mild pontine hypoplasia (arrow) (**A**). Axial T2 image shows frontal pachygyria/ polymicrogyria (PMG) (arrow), and PMG in temporal and insular areas (**B**). Axial FLAIR image shows splotchy white matter hyper-intensities (**C**). (**D-F**) P2. Small pons and small cerebellum (short arrow) in large cisterna magna, and thick tectum (long arrow) (**D**). Sagittal T2 coronal T2 (**E**) and axial T1 (**F**) views show hydrocephalus with thin or disrupted corpus callosum and missing septum pellucidum, abnormal gyration. (**G**) P3. Sagittal T1 view

shows oxycephalic shape; a shunt track is noted (arrow). The corpus callosum is absent; there is a “kinked” hypoplastic brainstem with small and flat pons. The occipital lobe and cerebellum are inferiorly displaced. (**H**) P3. Coronal T1 sequence shows abnormal sulcation of the brain cortex. (**I**) P3. DL: axial fast recovery fast spin echo T2 view shows short antero-posterior diameter of the head. T2 hyperintensities are present throughout the white matter. There is a thickened cortical mantle with irregular gray/white matter junction (arrowhead). There is also a band-like heterotopic layer under the abnormally formed occipito-parietal cortex (arrow). (**J**) P4. A sagittal T1 image shows hydrocephalus, disrupted corpus callosum and cystic outpouching of the cerebral mantle, frontal pachygyria/PMG, hypoplastic pons and thick tectum (arrowhead) and markedly hypoplastic cerebellum (arrow). (**K**) P4. Axial T1 image shows a dysplastic left eye involving lens and vitreous (arrowhead), temporal lissencephalic/polymicrogyric cortex (arrow) and small pons. (**L**) P4. Axial T1 image shows fronto-temporal pachygyria/PMG (arrow) and left cystic outpouching of the cerebral mantle (arrowhead).

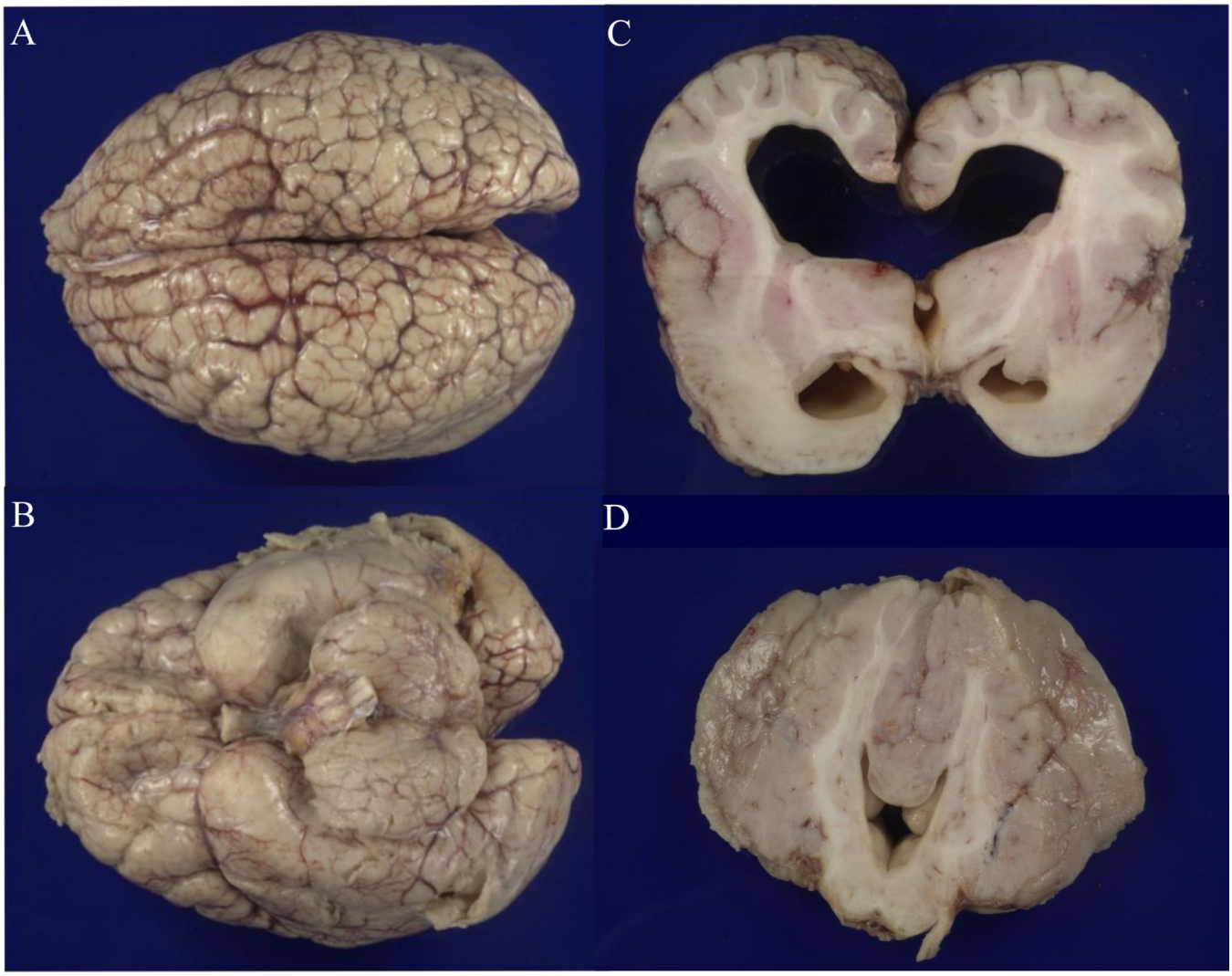

Figure 4.

Brain of patient P2. (**A**) Vertex view of cerebral hemispheres shows an abnormal gyral pattern resembling a “cobblestone” appearance. (**B**) Basal view of the brain shows a smooth, pachygyric cortex of the temporal lobes, abnormally smooth cerebellar folia, and hypoplastic brainstem. (**C**) Coronal section of the cerebrum at the level of the posterior limb of the internal capsule. Note the festooned cortical ribbon most prominent in the region of the Sylvian fissures bilaterally, the hypoplastic corpus callosum, absence of the septum pellucidum, fusion of the fornix, ventricular dilatation, and pachygyric temporal lobes. (**D**) Transverse section of the cerebellum and pons at the level of the exit of the 5th cranial nerve. Note the ‘molar tooth’ configuration of the 4th ventricle, hypoplasia of the basis pontis with a mild midline cleft, hypoplasia of cerebellar peduncles, relatively normal vermian folia, and pachyfolia of the hemispheres.

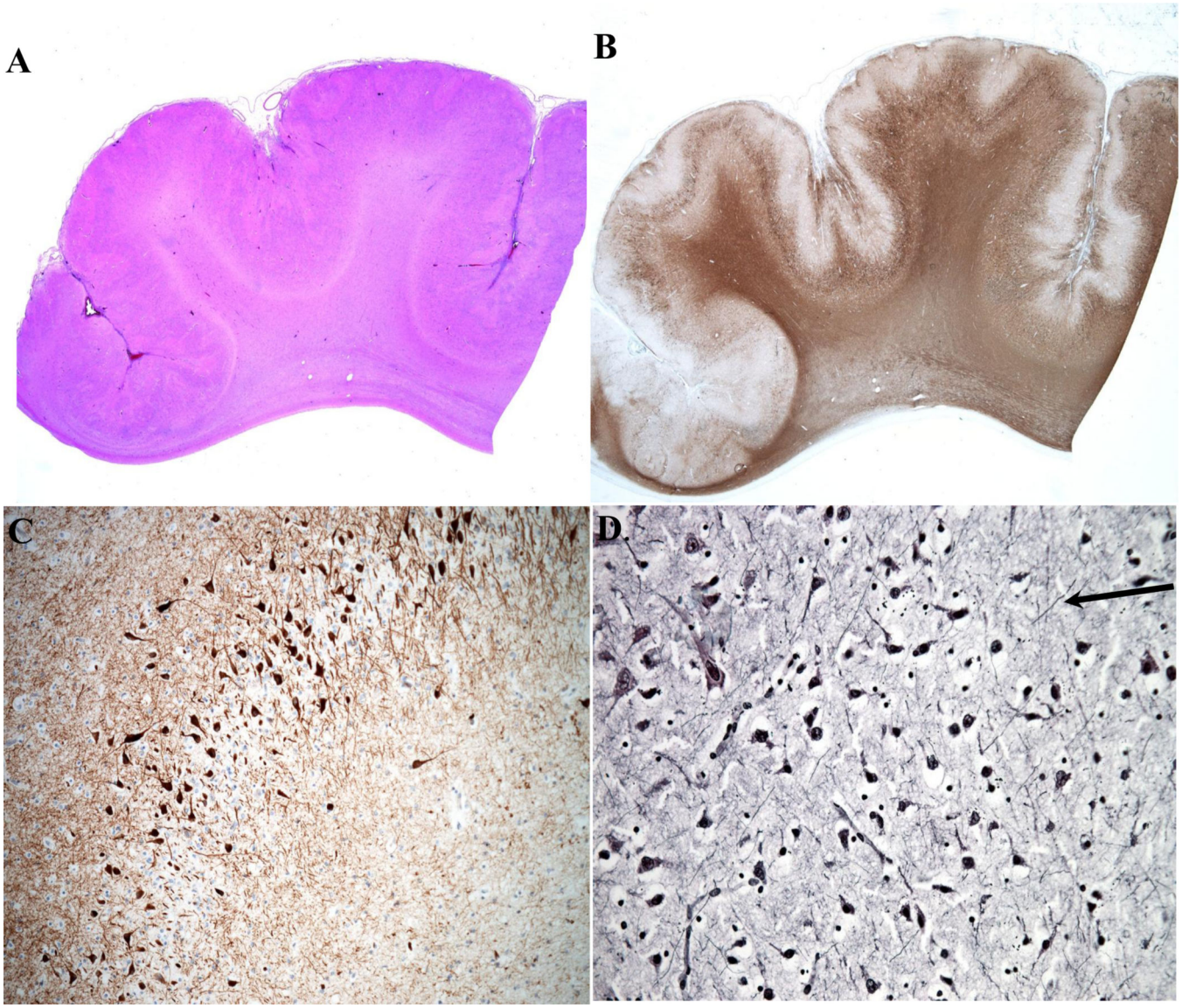

Figure 5.

Patient P2. (**A**) Section of frontal cortex shows festooned cortex typical of polymicrogyria. Note the minimal centrum semiovale; the wall of the ventricle parallels the cortex. H&E stain. Magnification: 2X. (**B**) Serial section of **A** immunostained for neurofilament protein (NFP) showing a paucity of neurons and abnormal lamination in the cortical ribbon. Immunohistochemistry preparation for NFP. Magnification: 2.5X. (**C**) NFP immunostain of the frontal cortex displays clustered disordered pyramidal neurons and no evidence of a 6-layered pattern. NFP. Magnification: 250X. (**D**) Section of frontal cortex shows disoriented neurons and delicate randomly distributed axons (arrow). Bodian silver technique. Magnification: 400X.

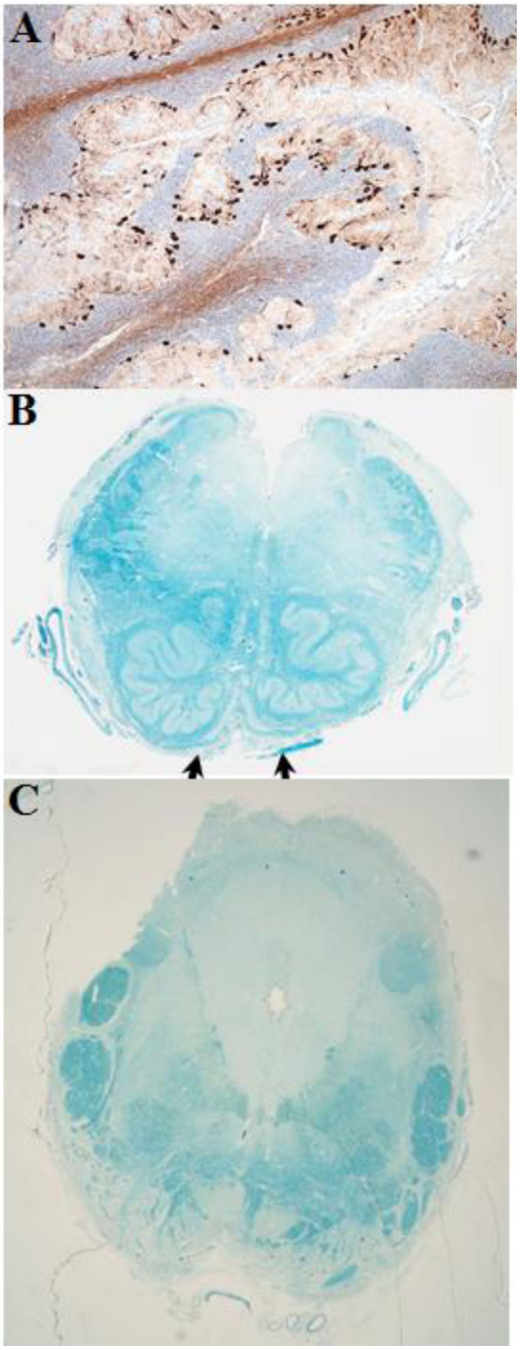

Figure 6.

Patient P2. (**A**) Cerebellar hemisphere folia show a lack of separation and disorganized architecture. Darkly stained cells are disordered Purkinje cells adjacent to pale blue swaths of internal granular neurons. Immunohistochemistry for neurofilament protein (NFP). Magnification: 250X. (**B**) Section of medulla showing absence of medullary pyramids (arrows). Klüver-Barrera stain. Magnification: 2X. (**C**) Section of midbrain showing excessive tegmental volume and aberrant large bundles of myelinated fibers on each side. Klüver-Barrera stain. Mag.: 10X.

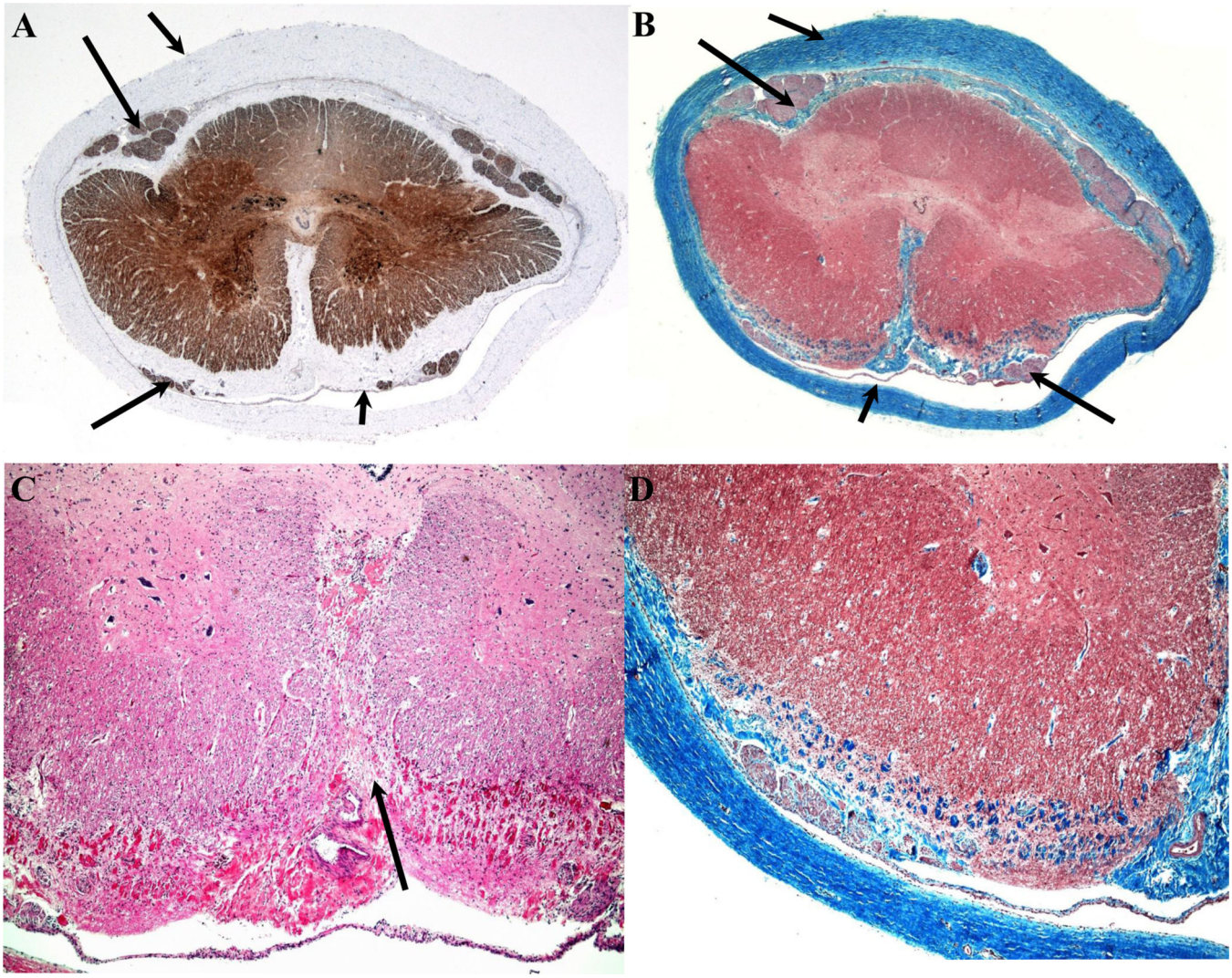

Figure 7.

Patient P2. (**A**) Transverse section of the cervical spinal cord displaying a “sombrero hat” configuration consequence to the absence of descending cortical spinal tracts. Note the markedly thickened pial layer, particularly ventrally, and the almost total obliteration of the subarachnoid space. Short arrow indicates arachnoid. Long arrows indicate anterior and posterior roots. Medium length arrow indicates the thickened dura. Immunohistochemistry for neurofilament protein. Magnification: 5X. (**B**) Trichrome stain of the cervical spinal cord showing thick dura (medium length arrow), thick fibrocollagenous tissue with only partial preservation of arachnoid (short arrow) and entrapped nerve roots (long arrows). Short arrow indicates the arachnoid. Adhesions are intermixed with spinal cord tissue. Magnification: 5X. (**C**) Ventral medial spinal cord showing a portion of anterior horns and white matter. The cell layer at the lower edge is arachnoid. Note the striking collagenization with incorporation of neural tissue along the ventral border and obliteration of the ventral fissure (arrow). H&E stain. Magnification: 100X. (**D**) Trichrome stain at the same level illustrates the intermixing of collagen (blue) with neural tissue (red). Magnification: 100X.

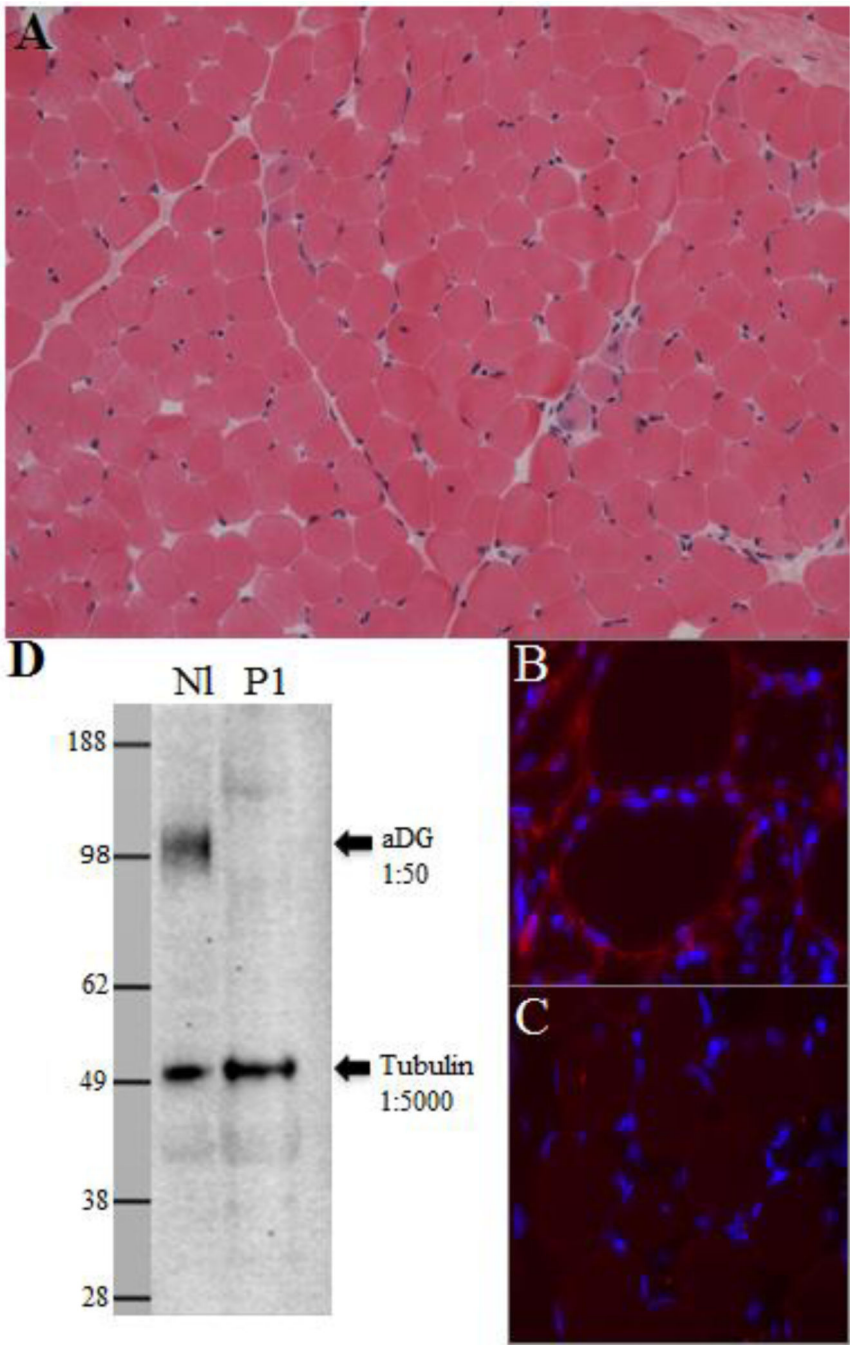

Figure 8.

Histology and immunohistochemistry and Western blot analysis of α-dystroglycan (αDG) in skeletal muscle tissue from patient P1. (**A**) H&E stain shows mild changes with occasional degeneration and regeneration but without excessive fibrosis. Magnification: 20X. (**B**) αDG staining with VIA41 (red) in the muscle of a healthy adult. Magnification: 40X. (**C**) αDG staining is reduced in P1. Magnification: 40X. (**D**) Immunoblot analysis of homogenates from muscle obtained from P1 and a healthy adult (NL). Abnormalities in αDG are

indicated by absent staining with antibody VIA41, which binds to glycosylated epitopes on αDG.

Table 1

Neurological Examination Findings

Neurological Exam	Patient 1 (age 7 y)	Patient 2 (age 9 mo)	Patient 3 (age 3 y)	Patient 4 (age 6 mo)
Mental Status	Awake, alert	Not aware of environment	Not aware of environment	Not aware of environment
Motor Development	Mild to moderate delay	Profound delay	Profound delay	Profound delay
Cognition and speech	Mild to moderate delays	Profound delays	Profound delays	Profound delays
Cranial Nerves	Mild eye esotropia with broken pursuit	Dysconjugate gaze, facial hypotonia	4mm pupils with brisk reaction, does not react to visual threat	Blindness, frequent choking
Strength (Medical Research Council Scale)	Mildly decreased, grade 4+ throughout	Decreased, grade 3-4 throughout	Decreased, 2 throughout	Decreased, grade 3-4 throughout
Muscle Bulk	Prominent calves and quadriceps	Decreased throughout	Normal	Normal
Muscle Tone	Mild generalized hypotonia	Severely hypotonic with truncal hypotonia	Severe generalized hypotonia, head lag	Severe generalized hypotonia, head lag
Range of motion	Tight heel cords bilaterally	*Fixed flexion at the MPJs of the hands with extension of the IPJs	Contractures of knees, ankles, fingers, hips	Knee contractures
Deep tendon reflexes	Mildly decreased on left	Decreased throughout	Absent throughout	Decreased throughout
Gait	Slightly slow and awkward but able to walk, run and clear the floor with both feet	Non-ambulatory	Non-ambulatory	Non-ambulatory
Coordination	No tremor or dysmetria	Not able to assess	Not able to assess	Not able to assess
Cardiac	Negative	Negative	Negative	Negative
Pulmonary	Negative	Coarse respirations, wheezing, tachypnea due to pneumonia	Negative	Negative
Other	Able to ascend (one hand hold) and descend (two hand hold) stairs, completed the 10-meter walk in 4.56 seconds and 4 steps in 3.15 seconds	Unusual features include sloping forehead with prominent metopic suture; synophrys; depressed nasal bridge with wide tip; tented upper lip with downturned corners of the mouth; midline upper alveolar notch; numerous scattered hyperpigmented macules supple neck, barrel shaped chest, gastroesophageal reflux	Seizures, scoliosis, splenic dysfunction; status post VP shunt for congenital hydrocephalus, Nissen fundoplication, G-tube placement, and tracheostomy; complete retinal detachment in right eye, poor retinal development in left eye with pale disc	Status post VP shunt for congenital hydrocephalus, NG tube feeding dependent, bilateral retinal detachment

*MPJ = Metacarpophalangeal joint, IPJ = Interphalangeal joint.

Table 2

Summary of Case Reports of *LARGE* Mutations

Reference	Case	Mutation	Phenotype	Brain MRI/CT	CK	Max motor ability	Eye involvement
(32)	Single female	c.1999insT (p.693X), c.1525G>A (p.Glu509Lys)	MEB/FCMD	Symmetrical white matter changes in periventricular region to the arcuate fibers in anterior and temporal regions, abnormal neuronal migration (similar to cobblestone complex), hypoplastic brainstem, mild pachygyria, thick and dysplastic cortex in frontal lobes with simplified gyri, shallow sulci	467-4500	Walking	Nystagmus
(37)	Single patient	Heterozygous c.1548C>G (p.Trp516X)	WWS	Hydrocephalus, white matter abnormality, cerebellar hypoplasia, lissencephaly	5700	None	Retinal detachment
(38)	Single patient	Heterozygous c.253_259dup (p.Gln87fs) Het c.992C>T (p.Ser331Phe)	MEB-like	Ventricular dilatation, white matter cortical changes, cerebellar cysts dysplastic cerebellar vermis, posterior concavity of the brainstem, pontine hypoplasia with cleft, frontoparietyal polymicrogyria	elevated	MEB-like with cerebellar cysts	Myopia
(39)	Brother, sister (+CS)	Homozygous 63 kb del (intron 8-10) resulting in premature stop codon	WWS	Dilatation of the lateral and third ventricle, Dandy-Walker malformation, absent inferior cerebellar vermis, hypoplastic cerebellum	1086-28,600	None	Bilateral leukocornia, retinal dysplasia, posterior synechia
(40)	Single patient	Homozygous c.1483T>C (Trp495Arg)	WWS	“WWS”	10X	Head control	NR
(27)	Two sisters (+CS)	Homozygous insertion between exons 10 and 11 and deletion in intron 10 of 3-4kb	Mild MEB	Cerebellar atrophy, particularly vermis, cerebellar cysts, mild generalized cerebral and pontine atrophy, dilatation of all ventricles, pachygyria of frontal lobes, white matter abnormalities (increased signal)	30-60X	Climbing stairs with difficulty	Mild myopia, strabismus
(41)	Two related fetuses	c.871+27358_1132-21850del42152insT; 252kb dup of exons 2-4	WWS	Severe quadriventricular hydrocephalus, cerebellar hypoplasia, agyria, thickened leptomeninges filled with neuroglial ectopia, disorganized cortical ribbon with multiple gaps in glia limitans	NR	NR	Bulging eyes, horizontal narrow palpebral slit
(41)	Single fetus	c.106+6361_408-6628del122058insGTGTG; c.615+24218_788-42869del105083insAATG	WWS	Triventricular hydrocephalus, agyria, thickened leptomeninges filled with neuroglial ectopia, disorganized cortical ribbon with multiple gaps in glia limitans, cerebellar dysplasia	NR	NR	No retinal dysplasia or other eye involvement
Patient 1 this report	Single female	74 kb deletion flanking exons 4-6, c.1525G>A, (p.Glu509Lys)	FCMD	Pachygyria/polymicrogyria in frontoparietal distribution, patchy white matter signal abnormalities in higher parietal white matter slightly small pons, inferior vermis hypoplasia,	2230	Running	Amblyopia, microtropia

Reference	Case	Mutation	Phenotype	Brain MRI/CT	CK	Max motor ability	Eye involvement
Patient 2 this report	Single female	Homozygous c.1328_1329 delGCinsAT (p.Cys443Tyr)	WWS	Hydrocephalus, absent septum pellucidum, smooth cortical surface in particular of the temporal lobes and the occipital lobes, with shallow gyration of the frontal and dorsal brain surface, very small pons and atrophic cerebellum with cerebellar cysts	3099-6620	None	Dysconjugate gaze, thin optic nerves, optic nerve disc, diminished diameter, severe atrophy of the ganglion cells and of the nerve fiber layer, which at the margin of the optic disc only had one-third of the normal thickness and contained glial nuclei.
Patient 3 this report	Single male	330.6kb deletion of exons 3-7; 74.3kb deletion of exon 7	WWS	Hydrocephalus s/p VP shunt, white matter hypointensities on T1 frontally and temporally, widespread pachygyria/polymicrogyria frontally and posteriorly, small pons, thick tectum, abnormal cerebellum, absent corpus callosum, double heterotropic layer posteriorly	6021-6702	None	Complete retinal detachment on right causing retinal atrophy and dialysis inferotemporally, poor retinal development on left with pale disc, pigmented atrophy in the central macula with traction along inferotemporal arcade, bilateral optic atrophy
Patient 4 this report	Single male	108kb homozygous deletion of exons 4-7	WWS	Hydrocephalus s/p VP shunt, disrupted corpus callosum, thick tectum, pachygyria/polymicrogyria, hypoplastic pons, hypo- and dysplastic cerebellum	4668	None	Bilateral retinal detachment and blindness, dysplastic left eye involving vitreous and lens

CK, creatine kinase; CS, consanguinity; FCMD, Fukuyama Congenital Muscular Dystrophy; MEB, Muscle Eye Brain Disease; MRI, magnetic resonance imaging; NR, not reported; WWS, Walker Warburg Syndrome.

Table 3

Summary of Immunohistochemical Characterization of Frontal and Temporal Cortical Laminar Organization in the Brain of Patient P2

Antigen	Normal laminar labeling	Frontal cortex	Temporal cortex
Reelin	Cajal-Retzius neurons in layer 1	In marginal layer and most abundant in fused gyri	Diffusely distributed
TBRI	Predominately layer 6	Primarily in subplate	Diffusely distributed
CTIP2	Neurons in layers 2,3,5	Distributed in bands	Diffusely distributed
SatB2	Predominately neurons in layers 2 and 3	Distributed in all layers	Diffusely distributed

* Cortical neuron laminar organization was characterized in the laboratory of Dr. Jeffrey Golden (35).

TBR1, transcription factor T-Box, brain, 1; CTIP2, Chicken ovalbumin upstream promoter transcription factor-interacting protein 2; SatB2, Special AT-rich sequence-binding protein 2.

Table 4

Neurocognitive Testing Results for Patient P1

Test	Score*	Percentile
Wechsler Nonverbal Scale of Ability		
Matrices	T = 10	<1
Coding	T = 10	<1
Object Assembly	T = 30	2
Recognition	T = 10	<1
Full Scale WNV	T = 37	<.1
Peabody Picture Vocabulary Test-4	Std Sc = 60	.4
WPPSI-III Naming Subtest	Sc S = 3	1
Parent Scales		
Child Behavior Check List		
Internalizing Problems	T = 52	58
Externalizing Problems	T = 62	89
Total Problems	T = 63	90
Social Communication Questionnaire	Total = 14	WNL
Social Responsiveness Scale	T = 78	99
Vineland Adaptive Behavior Scales-II		
Communication	Std Sc = 61	<1
Daily Living Skills	Std Sc = 77	6
Socialization	Std Sc = 66	1
Motor Skills		

T- score mean = 50 ±10; Std Sc mean = 100 ±; ScS mean = 10 ± 3.

WPPSI III, Wechsler Preschool and Primary Scale of Intelligence-Third Edition ; WNL, within normal limits.